Available online at www.sciencedirect.com
ScienceDirect
Ceramics International 37 (2011) 3281–3289
CERAMICS INTERNATIONAL
www.elsevier.com/locate/ceramint

Conversion of wooden structures into porous SiC with shape memory synthesis

Rajnish Dhiman [a], Victor Petrunin [a], Kuldeep Rana [b], Per Morgen [a,*]

[a] Department of Physics and Chemistry, University of Southern Denmark, Campusvej 55, DK-5230 Odense M, Denmark
[b] Department of Chemistry, Bilkent University, Bilkent, 06800 Ankara, Turkey

Received 6 May 2011; accepted 23 May 2011
Available online 27 May 2011

Abstract

Synthesis of structured silicon carbide materials can be accomplished using wooden materials as the carbon source, with various silicon impregnation techniques. We have explored the low cost synthesis of SiC by impregnation of carbon from wood with SiO gas at high temperatures, which largely retains the structure of the starting wood (*shape memory synthesis*). Suitably structured, porous SiC could prove to be an important type of catalyst support material. Shape memory synthesis (SMS) has earlier been tried on high surface area carbon materials. Here we have made an extensive study of SMS on carbon structures obtained from different types of wood.

Keywords: B. Electron microscopy; B. X-ray methods; Carbon preforms; Mesoporous SiC structures; Shape memory synthesis

1. Introduction

Silicon carbide embodies some very useful properties like low mass density, high-thermal conductivity (350–490 $W\,m^{-1}\,K^{-1}$) [1], strong resistance towards oxidation, and high mechanical strength and hardness, which makes it a potential material for many industrial applications [2–4]. Crystalline or amorphous silicon carbide is a semiconductor material, which has some unique electrical and electronic qualities [1,5] facilitating applications at high temperatures, high frequencies, high fields, and high powers [6,7]. Materials with such properties and which, additionally, can be easily formed with meso- or nanoporosity, should also be strongly solicited for applications in catalysis, gas reforming reactions, sensors, biotechnology, fuel cells, for hydrogen storage, and as hydrogen sources [8].

Nowadays synthesizing ceramics and composites from biological materials [9,10] is attractive because it uses naturally abundant resources such as wood. Plants are also used as starting materials, and the resulting products, under certain conditions, nearly retain the shape of the original solid framework of the plants. Molten silicon impregnation [11–15] and silicon vapor impregnation [16] have been employed earlier to convert charcoal obtained from wood into SiC. But this process does not retain any porosity of the wooden material as it fills the pores with molten silicon. Silica, from impregnation of the wood with tetraethyl orthosilicate (TEOS), has been used as silicon precursor [9,17], preserving the porosity. Vogli et al. [18] converted oak wood to SiC replicas by a reaction with gaseous silicon monoxide. This particular type of processing of carbon with silicon monoxide is commonly known as ''shape memory synthesis''. Vogli et al. [18] at present is the only reported work synthesizing SiC using shape memory synthesis with carbon obtained from wood. In the present work, we have extensively used the shape memory synthesis method with the carbon structures obtained from different kind of woods for the synthesis of porous SiC elements. We report a detailed study of the mechanisms and the structural and compositional properties of the products, such as crystal structure, composition, and specific surface areas.

The shape memory synthesis method has already been shown feasible for producing high surface area SiC structures with various kinds of carbon elements such as activated carbon, carbon nano tubes etc. [2,19,20]. A localized chemical reaction takes place between SiO vapors and C-atoms everywhere on the carbon framework that results in liberation of CO gas and the

* Corresponding author. Tel.: +45 6550 3529; fax: +45 6550 3529.
E-mail address: per@ifk.sdu.dk (P. Morgen).

0272-8842/$36.00
doi:10.1016/j.ceramint.2011.05.124

formation of a nearly 1:1 replica of the entire structure as pure SiC. Due to the high temperatures used, the process tends to produce crystalline materials.

SiC possess the properties required for a good catalyst material. A good catalytic support material has a high specific surface area, high mechanical strength, high thermal stability and high conductivity. Alumina, silica and a carbon-based materials [2,21,22], are very often used as catalytic support materials, but against the criteria presented above for choices of catalytic materials, they are having some drawbacks [2]. Thus, Moene et al. [22,23] and Ledoux and co-workers [2,19–21,24–26] have already discussed the large potential in SiC as a support material. Moene et al. [22,23] have proven that high surface area (30 m^2/g) SiC shows an excellent thermal stability under non-oxidative conditions. They have thus measured SiC reactivity against those of silica and alumina [23]. Due to the highly porous honeycomb structure (as shown in SEM pictures) of our SiC samples, and their high specific surface area in the range of 11–21 m^2/g, it should be easy to use the incipient wetness impregnation method to prepare the catalyst on such SiC supports. Thus, the SiC samples synthesized in this work from carbon preforms obtained from wood are potentially valuable catalyst supports. These SiC samples contain many stacking faults and structural imperfections, as shown with X-ray diffraction (XRD) and Raman techniques. The SiC samples made here are easily crushed into powder form by milling and are therefore well suited for producing mixtures with transition metals in mechanical alloying processes. They could therefore be very useful for high velocity oxygen fuel (HVOF) thermal spray applications to deposit wear- and corrosion resistive SiC coatings. A high amount of defects is commonly considered to result in an enhanced chemical surface activity [27,28], making it easier to manufacture the metal matrix composites required for this application [29] in the form of metal-oxide and metal-carbide compounds of high strengths.

2. Experimental

Wooden samples were carved into rectangular blocks of different sizes roughly ranging from 10 mm to 15 mm in length, 7 mm to 10 mm in breadth and 5 mm to 8 mm in height, and their initial masses were measured. Different kinds of wood like Indian pine (*Pinus sp.*), Indian mango (*Mangifera indica*), Silk cotton tree (*Bombax ceiba*), Indian blackberry (*Syzygium cumini*), Cutch tree (*Acacia catechu*), Danish beech (*Fagus sylvatica*) were used. The samples were dried at a temperature of 70 °C for 2 h and then heated at a slow rate of 1 °C/min up to 500 °C. During this heating, polyaromatic hydrocarbon polymers like cellulose, hemicellulose and lignin completely decompose to carbon. After 500 °C, the samples were heated to 1200 °C at the heating rate of 5 °C/min and kept at the same temperature for 6 h for further crystallization and purification of the carbon structures. All the process steps were carried out in an argon flow in order to prevent the wood from burning. After this pyrolysis process, solidified carbon skeleton structures (also termed as carbon preforms) were obtained with the same shape as in the original wood but somewhat contracted from the original dimensions of the starting wood as shown in Table 1. The wood samples were characterized by thermogravimetric analysis (TGA) in an argon atmosphere with a flow rate of 50 ml/min to monitor the change in weight with variation of temperature. The carbon preforms were characterized by SEM, XRD, and Raman microscopy.

These carbon ''preform'' materials were then placed next to a uniform 1:1 molar mixture of silicon and silica powder in an alumina crucible inside an alumina tube lined tubular furnace. The gas induced reaction process is done with a temperature program in which the main part of the reaction happens in the temperature range of 1400–1450 °C in an argon flow, with a flow rate of around 250–300 ml/min, for 12–15 h.

The resulting SiC samples are characterized by X-ray diffraction (XRD) to detect the Si:C stoichiometry and their crystal structures, using a Siemens diffractometer D5000. The samples were also analysed for their topographical microstructure by using a LEO 435 VP scanning electron microscope (SEM), and the composition was checked by the energy dispersive X-ray technique (EDX) with a RONTEC detector attached to the same SEM. The confirmation of the silicon carbide structure is also done with a Raman microscope from Dilor, using the 514 nm Ar-ion laser line. For analyses of the surface compositions, X-ray photoelectron spectroscopy (XPS) is done with a SPECS PHOIBOS® 100 system. The surface area of the samples was checked with a Surface Areameter from Quantachrome.

Table 1
Changes in the dimensions of the wood after carburization.

Sample name	Loss in length/%	Loss in breadth/%	Loss in height/%	Loss in volume/%	Loss in weight/%
IP_3_8_CB	32.9	23.6	30.5	64.4	75.3
IM_3_8_CB	21.1	32.5	26.0	60.6	76.5
IS_3_8_CB	23.7	32.1	27.9	62.7	77.0
IBB_3_8_CB	29.4	37.5	22.8	65.9	79.5
IM_3_8_Si	21.6	26.8	35.2	62.8	76.8
IS_3_8_Si	21.9	34.7	33.9	66.3	79.1
USL1	21.3	22.7	46.1	67.2	77.3
USM1	21.6	37.9	35.2	68.4	78.1
US1	21.4	34.0	32.6	65.0	76.3
US2	22.0	36.1	36.7	68.5	75.5

3. Results and discussion

3.1. Conversion of wood to carbon preforms

The wooden structures were pyrolyzed in an argon atmosphere to obtain the solid carbon preforms, which were retained for further processing. Some shrinkage in the dimensions of the wood, and a weight loss, are observed during the pyrolysis of wood, as reported earlier [11,30–33]. Table 1 shows the percentage loss in dimensions, volume and weight of some of the selected samples. It is clearly indicated that wood loses around 20–35% of its length, breadth and height, which makes its volume loss 60–70%. Careful observation of the percentage loss of any of the linear dimensions indicates three categories. The first category has length losses of around 32–35%; the second has 25–27% and the third around 20–22% in each of the samples. This suggests that there is some preferred direction of shrinkage along axial, tangential or radial directions as observed in earlier works [11]. Table 1 shows a weight loss of around 75–80%. The shrinkage and weight losses can be attributed to the removal of volatile components like polyaromatic hydrocarbon polymers (cellulose, hemicellulose and lignin), which are known constituents of wood.

3.2. Thermogravimetric analysis (TGA)

The mass change during the conversion of wood to pure carbon was investigated using thermogravimetric analysis (TGA) as shown in Fig. 1. This measurement shows a significant change in the mass from 250 °C to 350 °C. The entire TG curve shows four stages. The first stage is from room temperature to 70 °C, the second from 200–250 °C to 250–500 °C as the third, and the fourth one is seen above 600 °C. The loss of moisture from the sample is responsible for the mass change in the first stage. The change from 200 to 250 °C, at a slower rate, is due to the removal of physically adsorbed water and other adsorbed atmospheric gases like nitrogen, oxygen etc. in the sample. The major mass loss occurs in the third stage from 250 °C to 500 °C. As reported in the literature [11,34], this can be understood as the decomposition of hemicellulose, cellulose and lignin, which are the prime soft constituents of wood, with respective decomposition temperatures of 280, 340 and 400 °C [35]. This means that wood started degrading at 250 °C. The major mass change has happened below 400 °C and only a slight loss is observed afterwards. After 600 °C the carbon structure starts rearranging [35] from broken –C–C– chains of biopolymer aromatic carbon structures to crystallites of the carbon preform. This process is responsible for the slow mass change in the fourth stage of the TG curve. There is roughly a 75–80% mass loss from the starting wood, which is different from the theoretical value of 50% of volatile components in wood and this extra loss may be due to the presence of moisture, adsorbed water and other gases, which are escaping mainly in the first and second phases of the TG curve. From Table 1 it is clear that the percentage mass loss of different samples varies, which is explained by the fact that different woods have different lignin to cellulose ratios and also different cellular structures.

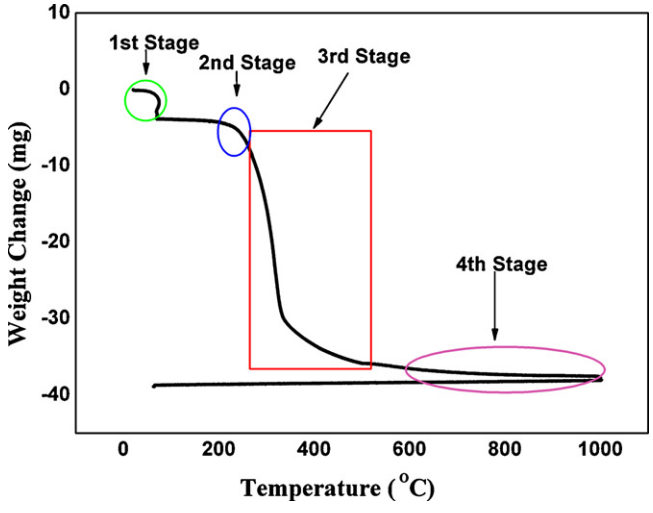

Fig. 1. TGA of a wood sample heated up to a temperature of 1000 °C in the presence of argon flow.

3.3. Characterization of the carbon preforms

Scanning electron microscopy (SEM) images of two different carbon preforms obtained from Danish beech and Indian pine are shown in Fig. 2(a and b), respectively. Flakes of carbon are broken off with the purpose of showing the inner structure of the carbon preforms. These figures clearly show the presence of capillaries inside the solid framework of the carbon preform, forming a honeycomb like structure. Different kinds of woods have different shapes and sizes of pores and capillaries. Danish beech wood has two kinds of pore structure with different sizes as shown in Fig. 2(a). Bigger pores have sizes in the range of 20-25 μm and smaller pores have sizes in the range of 5–8 μm. Fig. 2(b) shows a SEM image of Indian pine. It has relatively bigger pores than the Danish beech wood. This sample was cut at an oblique angle to the pore axes. Its structure is a well-ordered honeycomb structure. The pore size in case of Indian mango, silk cotton tree, and Indian blackberry is approximately identical and is in the range of 5–10 μm (as suggested by Figs. 5(a–c), which are of their SiC replicas). These open structures in the initial carbon preform helps in the conversion of carbon to SiC by facilitating SiO vapors to pass into and through the pores and to react with the carbon. These pores are also responsible for increasing the porosity and surface area and reducing the density of the processed samples.

Fig. 3(a) shows an X-ray diffraction pattern of the carbon preform. The peaks at $2\theta = 23.6^\circ$ and 43.8° are indexed as (0 0 2) and (1 0 1) peaks of 2H-graphite. From the shape and intensity of the peaks, an amorphous nature of the carbon as a whole is evident along with the presence of some small size graphitic crystallites. The presence of these small size crystallites is also confirmed by the presence of a G-band in the Raman spectrum of this sample; see Fig. 3(b). The crystallinity is due to rearrangement of broken –C–C– chains of

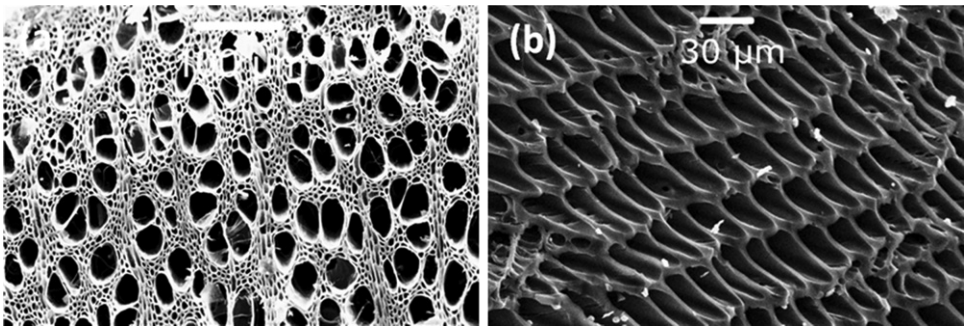

Fig. 2. SEM images of two carbon preforms obtained from (a) Danish beech and (b) Indian pine wood.

biopolymer aromatic carbon structures, which happens above 600 °C as explained in the discussion of the TGA results.

Fig. 3(b) shows the first order Raman spectrum of the carbon preform recorded in the region between 900 and 1900 cm^{-1}. The peaks appearing at 1590 and 1325 cm^{-1} are attributed to G and D-bands corresponding to peaks in crystalline graphite at 1582 and 1350 cm^{-1}, respectively [36,37]. The strong band at 1590 cm^{-1} corresponds to one of the E_{2g} modes (mode G) representing the movement of two neighboring carbon atoms opposite to each other in a graphene sheet. The 1325 cm^{-1} band is assigned to the D-mode, which is normally not a Raman active mode in graphitic carbon. Its occurrence here is attributed to defects and disorders. The FWHM of the G-band is around 99 cm^{-1}, which is much higher than the width for highly oriented pyrolytic graphite (HOPG) (15–18 cm^{-1} range). The Raman spectrum thus shows that the carbon preform contains amorphous carbon and some small size crystallites, in agreement with the XRD of the material shown in Fig. 3(a).

3.4. Determination of mass and density

After carburization of the wooden samples the resulting carbon preform structures were treated with the shape memory synthesis procedure.

In the *shape memory synthesis*, the SiO vapors react with carbon to form SiC as a product, while CO (*gas*) is liberated as byproduct. This reaction occurs in the temperature range of 1400–1450 °C. Silicon monooxide vapors are obtained by the reaction of silicon powder with silica powder at the same temperature as shown:

$$Si(solid) + SiO_2(solid) \rightarrow 2SiO(gas)$$

Then,

$$SiO(gas) + 2C(solid) \leftrightharpoons SiC(solid) + CO(gas)$$

Since this reaction is reversible in nature, the tube is flushed with streaming argon gas to remove the CO gas so the reaction proceeds in the forward direction. In this reaction, SiO vapors react randomly with carbon atoms to form SiC and CO gas, such that exactly half of the carbon atoms are replaced by silicon atoms, which may leave the shape of the preform unchanged. The expected mass (M) and density (D) of the samples are now calculated with this assumption using Eqs. (2) and (3):

$$M_{SiC} = \left(\frac{M_{carbon}}{2} + \frac{M_{carbon}}{2} \times \frac{28.0855}{12}\right) \quad (2)$$

$$D_{SiC} = \left(\frac{D_{carbon}}{2} + \frac{D_{carbon}}{2} \times \frac{28.0855}{12}\right) \quad (3)$$

From Table 2, we can see how the experimental and calculated values are in good agreement with each other. Small deviations in the density and masses of both the calculated and

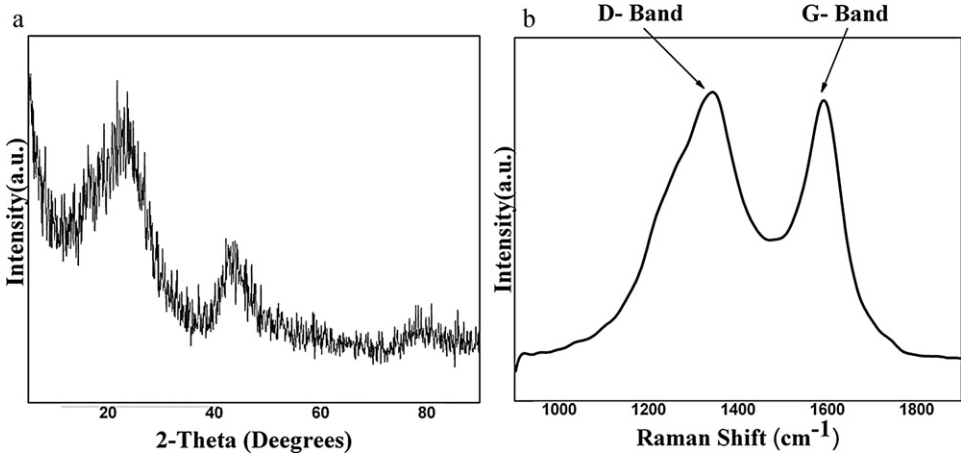

Fig. 3. (a) XRD pattern, and (b) Raman spectrum of a carbon preform obtained using the 514 nm excitation line.

Table 2
Calculated and experimental values of mass and density of the samples synthesized by SMS.

Sample name	Mass of carbon/g	Density of carbon/g cm^{-3}	Calcluated mass of SiC/g	Experimental mass of SiC/g	Deviation from calculated value of mass/%	Experimental value of density/g cm^{-3}	Calculated value of density/g cm^{-3}	Deviation from calculated value of density/%
IM_21_7	0.2049	0.29	0.3422	0.3332	2.6	0.467	0.480	2.6
IM_28_7	0.1549	0.33	0.2587	0.2509	3.0	0.558	0.549	−1.6
IM_3_8_Si	0.0696	0.31	0.1162	0.1200	−3.2	0.526	0.513	−2.5
IM_18_11-1	0.1161	0.33	0.1939	0.1818	6.3	0.53	0.557	4.9
IP_3_8_Si	0.1725	0.45	0.2881	0.2816	2.3	0.72	0.753	4.4
IS_3_8_Si	0.0354	0.25	0.0591	0.058	1.9	0.38	0.415	8.5
IBB_3_8_Si	0.0687	0.38	0.1147	0.1175	−2.4	0.646	0.638	−1.4
IBB_28_7	0.1407	0.44	0.2350	0.2314	1.5	0.724	0.743	2.5
DB_18_11-1	0.1217	0.35	0.2033	0.2005	1.6	0.093	0.096	3.0
DB_28_7	0.2153	0.34	0.3596	0.3341	7.1	0.556	0.575	3.2

Table 3
Percentage concentration of different polymorphs of SiC from XRD.

No.	Sample name	Cubic	2H	4H	6H	27R	29R
1	DB_18_11_9-2	37.5			62.5		
2	IM_3_8_CB	43.4	56.6				
3	DU_18_11-1	38.6			61.4		
4	IBB_28_7	40.3				59.7	
5	IBB_3_8_CB	25.2	73.1				1.7
6	IS_3_8_Si	59.4	40.6				
7	IM_28_7	40.4	52.7			6.9	
8	IP_3_8_SI	38.3			61.7		
9	IBB_28_7	40.3				59.7	

the experimental values can be attributed to errors in measuring the volume, the presence of heavy elements like calcium from the carbon preform, and the presence of the adsorbed atmospheric gases like nitrogen and oxygen in the samples, as confirmed by the EDX, XPS, and Auger results.

The samples retain the same amount of porosity as is present in the starting carbon preform and they are also observed to have a specific surface area of 11–21 m^2/g.

3.5. X-ray diffraction analysis

The crystallinity and polymorphism of the samples were checked with X-ray diffraction. The phase analysis of the diffraction patterns was done using the *X'pert High Score plus*™ software. The Rietveld refinement [38,39] technique was used to obtain accurate values of lattice parameters and phases present in the crystal structures. The samples are found to contain mixtures of α-SiC and β-SiC forms. The software calculates the percentage of different polymorphs in the samples. Table 3 summarizes the percentage distribution of different polymorphs of SiC in some of the synthesized samples.

The diffraction patterns of the samples are shown in Fig. 4. Considering the background in the XRD patterns, we can say that these samples are less crystalline than samples, we have

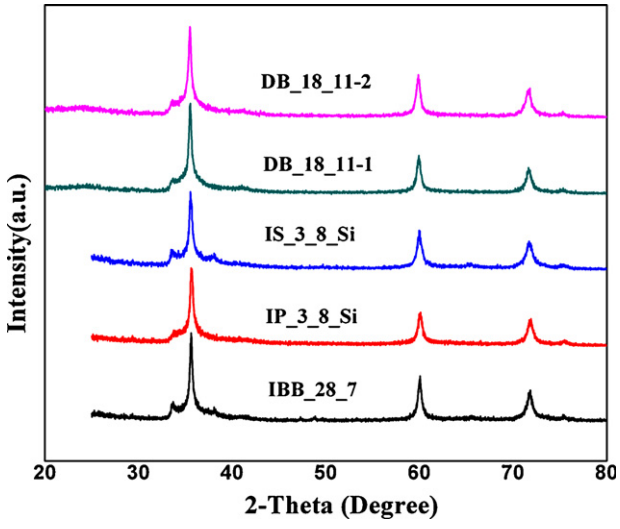

Fig. 4. XRD patterns of the samples.

made with the liquid silicon impregnation method in a parallel study. The present samples thus largely retain the structure of the original wood, i.e. anisotropic and amorphous and results in a higher XRD background in comparison to the samples synthesized by liquid silicon impregnation. The diffraction patterns of samples show the major peaks at $2\theta = 35.5^\circ$, 59.8° and 71.6°, which correspond to diffraction from SiC (1 1 1), SiC (2 2 0) and SiC (3 1 1) planes. Small shoulders at $2\theta = 33^\circ$ and 37.5° are also found which corresponds to α-SiC. From the results in Table 3, we can claim that the SMS always produces a mixture of α-SiC (2H, 4H, 6H, 27R, 29R etc.) and β-SiC (3C). The grain size of the samples varies in the range of 43–68 nm and the strain varies from 0.038 to 0.1%, as calculated by using the Williamson–Hall plot [40] from the XRD data.

3.6. Surface analysis of the samples

3.6.1. SEM and EDX analyses

The SEM images of the samples are shown in Fig. 5, which after comparison with Fig. 2 suggests that they retain the morphology of the starting carbon preforms. Pore structure and pore size of the samples synthesized from Indian blackberry, and silk cotton tree is almost the same as in Fig. 5(a and b). The samples were cut perpendicular to the pore axes in Fig. 5(a and b). Fig. 5(c) shows the SEM image of the Indian mango. This sample was cut parallel to the pore axes to show the capillary arrangement. Comparison of the SEM image of the carbon preform obtained from Danish beech wood in Fig. 2(b) with the SiC replica (Fig. 5(d)) confirms that the shape memory synthesis method preserves the initial shape, size and morphology of the carbon preform. Silicon carbide whiskers have also been observed over the top surface of the samples, which are similar to the ones observed in [41], where tetraethyl orthosilicate has been used as the silica precursor.

The EDX analysis shows Si, C, O, and Ca. Calcium was also found in the carbon preform of beech wood, taken up as nutrition [42]. A 6H–SiC wafer reference sample is used to calibrate the EDX system. The calculated atomic percentages of the synthesized sample were $39.5 \pm 0.4\%$ for silicon, $45.6 \pm 0.4\%$ for carbon, $10.8 \pm 0.3\%$for oxygen and $4.0 \pm 0.2\%$ for calcium.

Only 2.5% oxygen is detected on the 6H–SiC wafer, while the synthesized sample shows 10.8%. This suggests that oxygen is more prone to adsorb in the porous framework of the synthesized samples at high temperatures. Mapping of elements with EDX shows homogeneous distributions of silicon and carbon over the whole sample.

3.6.2. XPS analysis

XPS spectra of different samples are shown in Fig. 6. They are recorded from 200 eV to 1260 eV kinetic energy, excited with an Mg X-ray source (Mg K_α). They all show peaks of carbon, oxygen and silicon along with some other peaks such as (Ar 2p) and (N 1s) seen for the 6H–SiC wafer acting as a reference sample. This reference sample had initially been sputtered with argon for 30 min. There are also traces of calcium ($\approx$0.5% concentration) in the samples, which comes from the initial wooden precursor [42]. All samples have been analysed for the presence of carbon, silicon and oxygen. The samples get oxidized due to the handling in air for many days after the synthesis. The handling of the reference sample in the open air has also oxidized the 6H–SiC wafer, to a similar degree. The ratio of Si:C in the different samples scatter somewhat. The surface region (as measured by XPS) of the

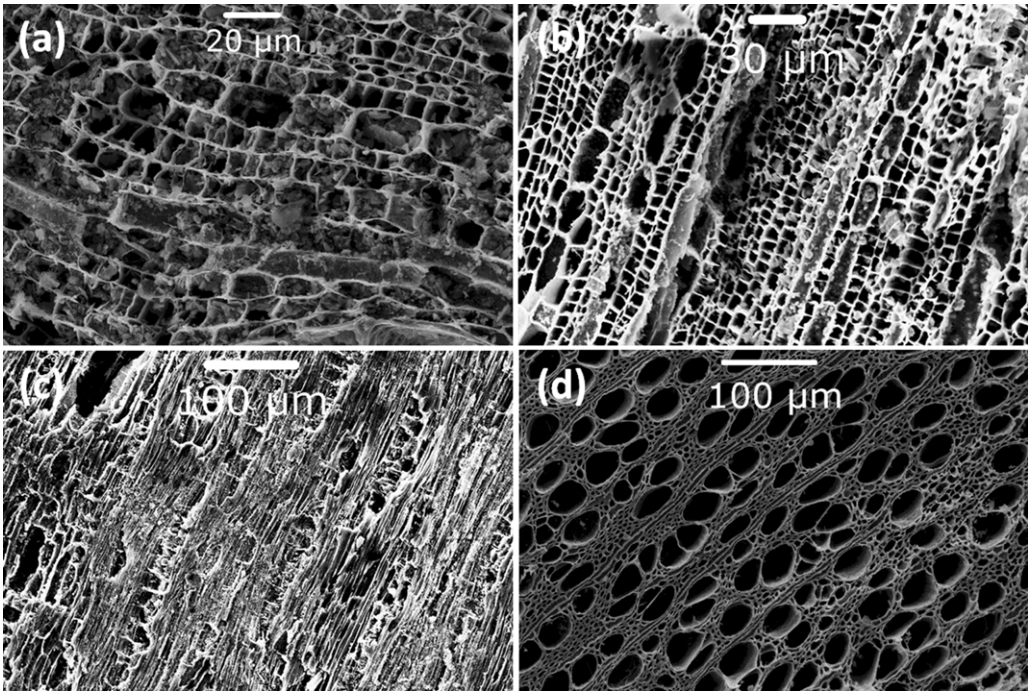

Fig. 5. Scanning electron microscopy of the SiC samples made from (a) Indian blackberry, (b) silk cotton tree, (c) Indian mango, and (d) Danish beech wood (compare Fig. 2(b)).

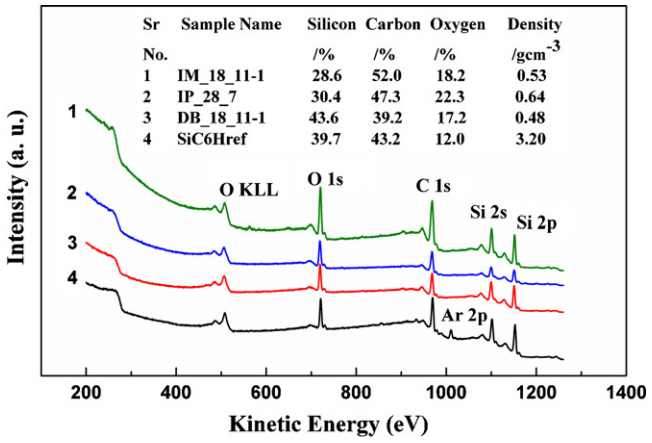

Fig. 6. XPS spectra of different samples along with the 6H–SiC reference sample. The inset table shows the percentage concentrations of the respective samples as calculated by the CasaXPS™ software.

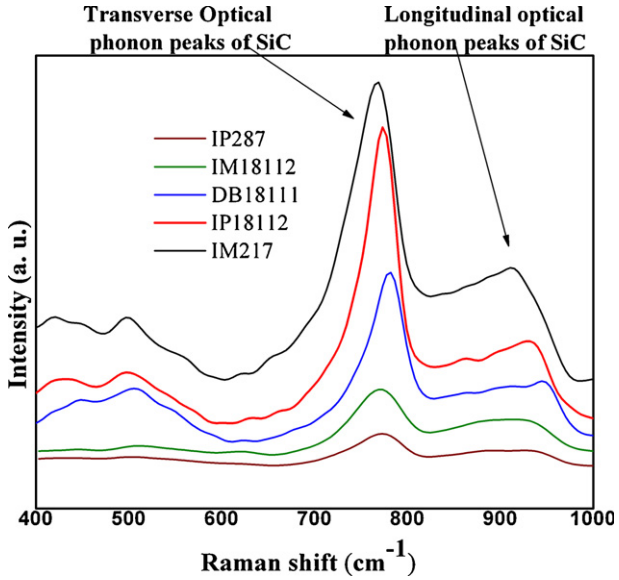

Fig. 7. Raman spectra of the samples.

samples is carbon rich except for one sample which is rather showing approximately 1:1 ratio of Si:C. The general shape of the wide scan XPS spectra varies with the density and structure of the samples. The inelastic background regions show a dependence on density and morphology. Thus, the reference 6H–SiC sample has the flattest background below the O 1s and O KLL peaks (at 720 eV and 500 eV), while the least dense and most porous samples made by shape memory synthesis show the highest background slopes. Different background slopes below the oxygen signals (lower kinetic energies) indicate differences in the in-depth distributions of oxygen in the samples. Higher slopes indicate deeper penetration of oxygen. From the XPS results in Fig. 6, we see that the top surface of the SiC samples is oxidized as (amorphous) SiO_2. The synthesized samples are all the time kept in the open after their synthesis in the non-reactive argon atmosphere (for comparison, a differently prepared standard reference sample with a nominal 1:1 stoichiometry gives a Si:C surface concentration ratio of 56%:44%, using the CasaXPS™ software).

Thus all samples studied here are definitely enriched in carbon at the surface, as received. This might be due to carbon contamination during handling, insertion and storage of samples in ultra high vacuum conditions.

3.7. Raman analysis

Raman spectroscopy is one of the most sensitive techniques for distinguishing between the different polymorphic types of SiC [43,44]. Silicon carbide is known to have a large number of polymorphs, of which β-SiC has a *zinc blende* kind of structure with the smallest unit cell of all the SiC polymorphs. Bulk β-SiC has two optical modes at the Γ point of the Brillouin zone, a transverse optic (*TO*) mode at 796 cm^{-1} and a longitudinal optic (*LO*) mode at 972 cm^{-1} [44]. These modes have different energies, which in "higher" polytypes can be used to distinguish the different polymorphs. We worked with the most commonly used 514 nm laser line for the Raman measurements and then compared our spectra with those in the literature [43] regarding both the position of Raman peaks and their intensity distributions.

Fig. 7 shows the Raman spectra of the samples; the corresponding peak positions are given in Table 4. The full widths at half maximum (FWHM) for these Raman lines are rather broad, in the range of 35–48 cm^{-1}, which suggests that they are having large number of stacking faults, as expected from the local poly-anisotropic nature of the starting wood. Due to this large FWHM we cannot determine the exact peak position of each sample and cannot claim the exact polymorph type with certainty, but simple association, in the table, makes some suggestions obvious. In Table 4, we can see that there are differences in the positions of the peaks and from the comparison with literature [43,44] it is suggested that these can be from 2H or 4H–SiC. These assignments are also supported by comparison with the XRD results for the amounts of different polymorphs in the samples as shown in Table 3.

Table 4
Peak positions in the Raman spectra of the samples and respective suggestions for the different polymorphs.

Sample name	Peak positions/cm^{-1} (± 4 cm^{-1})	Suggestions for polymorph/cm^{-1} [43,44]
IP_28_7	770.2, 886.3, 930.2	2H or 4H
IP_18_11_2	770.7, 861.5, 903.4, 935.9	2H or 4H
DB_18_11-1	777.8, 896.7, 956.8	4H (776 & 964)
IM_18_11_2	766.9, 897, 934	2H (764 & 968)
IM_21_7	763.6, 874.7, 917.5	2H (764 & 968)

Table 5
Specific surface area of the samples.

Sr. No.	Sample name	Type of starting wood	Surface area (m^2/g)
1	IM_3_8_CB	Indian mango	11.82
2	IM_7_10	Indian mango	17.01
3	IP_28_7	Indian pine	18.74
4	DB_18_11_1	Danish beach	19.66
5	DB_28_7	Danish beach	21.16

Thus from the above results we can say that the samples produced by the shape memory synthesis method are formed in different phases with respective percentages obtained from the XRD analysis. The higher FWHM of the peaks indicates the higher amount of stacking faults and structural imperfections that may result in enhanced surface activities.

3.8. Specific surface area

The specific surfacearea of the samples have been measured using the BET adsorption isotherm method. Initially, the samples are evacuated and out gassed at high temperature (350 °C). After cooling them down to liquid nitrogen temperature, nitrogen gas at variable pressures is used to obtain six points on the BET adsorption isotherm, from which the specific surface area is calculated. The specific surface areas of the different samples vary in the range of 11.82–21.16 m^2/g. Table 5 shows the specific surface area of the samples made from different woods. This table suggests that the specific surface area of samples made from all these different kinds of wood is almost comparable. This is followed by the fact that the density of carbon obtained from these different woods is also nearly equal (varying from 0.29 to 0.35 $g\,cm^{-3}$) as shown in Table 2. The ''nitrogen'' pore volume of one of the samples synthesized from Danish beech wood is 0.14 ml/cm^3 while pore volume determination using water until external wetting is perceived, shows a pore volume of 1.1 ml/g. Thus it can be concluded that SiC ceramic elements synthesized from these particular kinds of woods appear with approximately identical surface areas and cellular structures. With SMS the silicon atoms are thus replacing half of the carbon atoms and leaving the initial carbon framework intact in shape. This method gives a higher specific surface area than when the same samples are synthesized by impregnation with liquid silicon.

4. Conclusions

Porous SiC elements are successfully synthesized with natural wood as the starting material using the shape memory synthesis procedure. The SiC structures obtained contain mixtures of α-SiC and β-SiC. The density of the porous samples is roughly around 6 times less than the density of bulk SiC (3.21 gm/cm^3), showing that they preserve the porous structure. The samples made by shape memory synthesis have obvious applications as catalysis support materials due to their porous nature and relatively high specific surface areas (11–21 m^2/g). Since the SMS processed materials have structural imperfections, which enhance their surface activity, and make it easy to crush them into powder form, they may also be used in SiC – transition metal matrix alloys, made by mechanical alloying during milling of a mixture of SiC powder and metal. These alloyed particles are predicted to be highly useful for HVOF thermal spray applications, and in this way be used to deposit high endurance, wear- and corrosion resistant SiC surface coatings.

Acknowledgements

This work is supported by the Danish Ministry for Research and Innovation, through its program for Sustainable Energy and The Environment, with the grant to R. Dhiman, 2104-05-0073. The authors are grateful for advice and technical support from E. Skou, S. Tougaard, T. Warner, P. B. Hansen, D. Kyrping, and T. Sørensen at SDU; to N. Dam Madsen, and P. Hald, from The University of Aarhus, to Jens Rafaelsen from Aalborg University, and to S. Vikram Singh from The RISØ National Laboratory, Roskilde, Denmark.

References

[1] Z. Li, Z. Zhang, A. Meng, J. Guo, Large-area highly-oriented SiC nanowire arrays: synthesis, Raman, and photoluminescence properties, J. Phys. Chem. B 110 (2006) 22382–22386.
[2] J.M. Nihut, R. Vieira, L. Pesant, J.P. Tessonnier, N. Keller, G. Ehret, C.P. Huu, M.J. Ledoux, Synthesis and catalytic uses of carbon and silicon carbide nanostructures, Catal. Today 76 (2002) 11–32.
[3] J.A. Powell, L.G. Matus, M.A. Kuczmarski, Growth and characterization of cubic SiC single-crystal films on Si, J. Electrochem. Soc. 134 (1987) 1558–1565.
[4] W.J. Choyke, G. Pensk, Physical properties of SiC, Mater. Res. Soc. Bull. 22 (1997) 25–29.
[5] Z. Ju, X. Ma, N. Fan, P. Li, L. Xu, Y. Qian, High-yield synthesis of single-crystalline 3C–SiC nanowires by a facile autoclave route, Mater. Lett. 61 (2007) 3913–3915.
[6] A. Fissel, B. Schroter, W. Richter, Low temperature growth of SiC thin films on Si and 6H–SiC by solid source molecular beam epitaxy, Appl. Phys. Lett. 66 (1995) 3182–3184.
[7] Z.C. Feng, A.J. Mascarenhas, W.J. Choyke, J.A. Powell, Raman scattering studies of chemical vapor deposited cubic SiC films of (1 0 0) Si, J. Appl. Phys. 64 (1998) 3176–3186.
[8] G. Mpourmpakis, G.E. Froudakis, SiC nanotubes: a novel material for hydrogen storage, Nano Lett. 6 (2006) 1581–1583.
[9] A.V. Srinivasan, G.K. Haritos, F.L. Hedberg, Biomimetics: advancing man-made materials through guidance from nature, Appl. Mech. Rev. 44 (1991) 463–481.
[10] Y. Shin, C. Wang, G.J. Exarhos, Synthesis of SiC ceramics by the carbothermal reduction of mineralized wood with silica, Adv. Mater. 17 (2005) 73–77.
[11] P. Greil, L. Thomas, A. Kaindl, Biomorphic cellular silicon carbide ceramics from wood. I. Processing and microstructure, J. Euro. Ceram. Soc. 18 (1998) 1961–1973.
[12] P. Greil, L. Thomas, A. Kaindl, Biomorphic cellular silicon carbide ceramics from wood. II. Mechanical properties, J. Euro. Ceram. Soc. 8 (1998) 1975–1983.
[13] T. Ota, M. Takahashi, T. Hibi, M. Ozawa, S. Suzuki, Y. Hikichi, Biomimetic process for producing SiC from wood, J. Am. Ceram. Soc. 78 (1995) 3409–3411.
[14] O.P. Chakrabarti, H.S. Maiti, R. Majumdar, Si–SiC ceramics from plant precursor, J. Mater. Sci. 39 (2004) 4715–4717.

[15] D.W. Shin, S.S. Park, Y.H. Choa, K. Niihara, Silicon/silicon carbide composites fabricated by infiltration of a silicon melt into charcoal, J. Am. Ceram. Soc. 82 (1999) 3251–3253.
[16] E. Vogli, H. Sieber, P. Greil, Biomorphic SiC–ceramic prepared by Si-vapor phase infiltration of wood, J. Euro. Ceram. Soc. 22 (2002) 2663–2668.
[17] J. Locs, L.B. Cimdina, A. Zhurish, D. Loca, Optimized vacuum/pressure sol impregnation processing of wood for the synthesis of porous, biomorphic SiC ceramics, J. Euro. Ceram. Soc. 29 (2009) 1513–1519.
[18] E. Vogli, J. Mukerji, C. Hoffman, R. Kladny, H. Sieber, P. Greil, Conversion of oak to cellular silicon carbide ceramic by gas-phase reaction with silicon monoxide, J. Am. Ceram. Soc. 84 (2001) 1236–1240.
[19] N. Keller, O. Reiff, V. Keller, M.J. Ledoux, High surface area submicrometer-sized β-SiC particles grown by shape memory synthesis method, Diamond Relat. Mater. 14 (2005) 1353–1360.
[20] N. Keller, V. Keller, F. Garin, M.J. Ledoux, A new TiO_2–β-SiC material for use as photocatalyst, Mater. Lett. 58 (2004) 970–974.
[21] N. Keller, C.P. Huu, S. Roy, M.J. Ledoux, Influence of the preparation conditions on the synthesis of high surface area SiC for use as a heterogeneous catalyst support, J. Mater. Sci. 34 (1999) 3189–3202.
[22] R. Moene, M. Makkee, J.A. Moulijn, High surface area silicon carbide as catalyst support characterization and stability, Appl. Catal. A: Gen. 167 (1998) 321–330.
[23] R. Moene, E.P.A.M. Tijsen, M. Makkee, J.A. Moulijn, Synthesis and thermal stability of Ni, Cu, Co, and Mo catalysts based on high surface area silicon carbide, Appl. Catal. A: Gen. 184 (1999) 127–141.
[24] C.P. Huu, C. Bouchya, T. Dintzer, G. Ehret, C. Estournes, M.J. Ledoux, High surface area silicon carbide doped with zirconium for use as catalyst support. Preparation, characterization and catalytic application, Appl. Catal. A: Gen. 180 (1999) 385–397.
[25] M. Benaissa, P.H. Cuong, J. Werckman, C. Crouzet, M.J. Ledoux, A sub-nanometer structural study of Pt–Rh catalysts supported on Ce doped SiC, Catal. Today 23 (1995) 283–298.
[26] P.H. Cuong, S. Marin, M.J. Ledoux, M. Wiebel, G. Ehret, M. Benaissa, E. Peschiera, Synthesis and characterization of platinum–rhodium supported on SiC and SiC doped with cerium: catalytic activity for the automobile exhaust reactions, Appl. Catal. B Environ. 4 (1995) 45–63.
[27] C. Jia, Z. Li, Z. Xie, A research on detonation gun coating with Fe–SiC composite powders mechanically activated, Mater. Sci. Eng. A 263 (1999) 96–100.
[28] H. Ferkel, Properties of copper reinforced by laser-generated Al_2O_3-nanoparticles, Nanostruct. Mater. 11 (1999) 595–602.
[29] J. Pelleg, Reactions in the matrix and interface of the Fe–SiC metal matrix composite system, Mater. Sci. Eng. A 269 (1999) 225–241.
[30] C.E. Byrne, D.C. Nagle, Carbonization of wood for advanced materials applications, Carbon 35 (1997) 259–266.
[31] T. Hata, Microstructural analysis of biocarbon from wood, Cellulose Commun. 6 (1999) 127–133.
[32] O. Paris, C. Zollfrank, G.A. Zickler, Decomposition and carbonisation of wood biopolymers – a microstructural study of softwood pyrolysis, Carbon 43 (2005) 53–66.
[33] G.A. Zickler, W. Wagmaier, S.S. Funari, M. Burghammer, O. Paris, In situ X-ray diffraction investigation of thermal decomposition of wood cellulose, J. Anal. Appl. Pyrolysis 80 (2007) 134–140.
[34] P. Ehrburger, L. Lahaye, E. Wozniak, Effect of carbonization on the porosity of beechwood, Carbon 20 (1982) 433–439.
[35] F. Shafizadeh, Y. Sekiguchi, Development of aromaticity in cellulosic chars, Carbon 21 (1983) 511–516.
[36] G. Maurin, F. Henn, B. Simon, J.F. Colomer, J.B. Nagy, Lithium doping of multiwalled carbon nanotubes produced by catalytic decomposition, Nano Lett. 1 (2001) 75–79.
[37] H. Hiura, T.W. Ebbesen, K. Tanigaki, H. Takahashi, Raman studies of carbon nanotubes, Chem. Phys. Lett. 202 (1993) 509–512.
[38] C.L. Burdick, E.A. Owen, The atomic structure of carborundum determined by X-rays, J. Am. Chem. Soc. 40 (1918) 1749–1759.
[39] P.T.B. Shaffer, A review of the structure of silicon carbide, Acta Crystallogr. B 25 (1969) 477–488.
[40] G.K. Williamson, W.H. Hall, X-ray line broadening from filed aluminium and wolfram, Acta Metall. 1 (1953) 22–31.
[41] R. Dhiman, P. Morgen, Growth of SiCnano-whiskers on powdered SiC, nanotechnological basis for advanced sensors, NATO Science for Peace and Security Series B: Physics and Biophysics (2011) 281–285. , doi:10.1007/978-94-007-0903-4_31, Part 8.
[42] J. Fromm, Wood formation of trees in relation to potassium and calcium nutrition, Tree Physiol. 30 (2010) 1140–1147.
[43] S. Nakashima, M. Higashihira, K. Maeda, Raman scattering characterization of polytype in silicon carbide ceramics: comparison with X-ray diffraction, J. Am. Ceram. Soc. 86 (2003) 823–829.
[44] M. Bechelany, A. Brioude, D. Cornu, G. Ferro, P. Miele, A Raman spectroscopy study of individual SiC nanowires, Adv. Funct. Mater. 17 (2007) 939–943.